

NANOMATERIAL SYNTHESIS AND NANODEVICE FABRICATION BY LASER
CHEMICAL PROCESSING

by

Jing Shi

A dissertation

Presented to the faculty of
The Graduate College at the University of Nebraska
In Partial Fulfillment of Requirements
For the Degree of Doctor of Philosophy

Major: Engineering (Electrical Engineering)

Under the Supervision of Professor Yongfeng Lu

Lincoln, Nebraska

August, 2006

UMI Number: 3302727

PREVIEW

UMI[®]

UMI Microform 3302727

Copyright 2008 by ProQuest Information and Learning Company.
All rights reserved. This microform edition is protected against
unauthorized copying under Title 17, United States Code.

ProQuest Information and Learning Company
300 North Zeeb Road
P.O. Box 1346
Ann Arbor, MI 48106-1346

NANOMATERIAL SYNTHESIS AND NANODEVICE FABRICATION BY LASER CHEMICAL PROCESSING

Jing Shi, Ph. D.

University of Nebraska, 2006

Adviser: Yongfeng Lu

The main objective of this dissertation is to explore the possibility and extend the capability of laser-technology into nanoscale material processing. The research focused on three novel laser chemical processing techniques for nanomaterials processing, including 1) near-field-induced spatially-confined photochemical deposition of diamond-like carbon (DLC) films on nanostructures; 2) pulsed-laser disintegration of inorganic compounds as nanocatalysts for large-area carbon nanotube (CNT) growth; and 3) laser-assisted chemical vapor deposition (LCVD) growth of CNTs and direct fabrication of CNT field-effect transistors.

In the study of near-field induced photochemical deposition of DLC films on nanostructures, DLC was deposited on tungsten nanotips as well as Mo nanowedges using benzene as the precursor. Theoretical as well as experimental results confirmed the prediction of spatially confined and phase graded deposition of DLC film on sharp edges due to local intensity gradient of optical near field. We also developed a method to produce nanocatalysts by irradiating dispersed NiSO_4 microclusters on silicon substrates using a KrF excimer laser. Under appropriate laser fluences and multiple laser pulses, the disintegrated NiSO_4 nanocatalysts were used for large-area uniform multi-walled carbon nanotube (MWNT) growth. In the study of LCVD synthesis of CNTs, we have developed controlled synthesis of vertically-aligned CNFs, large-area high-quality MWNTs, and defect-free single-walled nanotubes (SWNTs) with different catalysts, carbon feedstock, and laser parameters. The synthesis could be achieved by both far-infrared CO_2 laser (10.6 μm) and near-infrared Nd:YAG laser (1064 nm) in a localized manner. The LCVD technique was also applied for direct fabrication of field-effect devices. Due to the unique advantages of the LCVD process, such as fast and local heating, as well as its potential to select chiralities during the growth, it may provide new features and versatilities in device fabrications.

DEDICATION

This dissertation is dedicated to Mom, Dad and my wife, Linna with love.

PREVIEW

ACKNOWLEDGEMENTS

Throughout my PhD research projects, I have obtained assistance from many people whom I want to deliver my sincere gratitude to. First of all, I want to thank my advisor, my mentor, Prof. Yongfeng Lu. He not only guided me through the PhD studies, but also showed me the real fervor and perseverance in research. Most of all, from him I learned how to be a self-motivated and self-sufficient person to deal with the future challenges and difficulties.

I also appreciate our project partners, Yushun Lin, Zhang Rui, and Prof. Sy-Hwang Liou from the Department of Physics and Astronomy for their contributions in lithography, sputtering and focused-ion beam experiments. Their diligence and kindness helped me through the projects.

I would also like to thank Prof. Dennis Alexander, Dr. Dave Doerr, Prof. Natale Ianno, Prof. Dan Thompson, and Prof. Rodney Soukup. I am deep indebted to them for their generous and continuous assistances in the experiments and helpful talks from various aspects in laser and materials. In addition, I will thank Prof. Xinwei Wang from the Department of Mechanical engineering for his instructive talks on thermal problems of laser material processing and his contribution of CO₂ laser for my LCVD project. I also appreciate Prof. Paul Snyder for his advices in material problems.

I also want to thank Dr. You Zhou, Dr. Kit Lee, and Dr. Gui Chuan Hou from the School of Biological Sciences for FESEM and EDX measurements, Dr. Lanping Yue from the Department of Physics and Astronomy for SPM measurements, Dr. Young Sik Kim from the Department of Material Science and Engineering, Iowa state University for micro-Raman measurements, and Dr. Stuart McKernan from IT Characterization Facility, University of Minnesota for HRTEM measurements.

I gained a lot of assistances and supports from many friends and colleagues too. Here I would like to deliver the sincere gratitude to Kiran Mendu, Lipan Li, Ravi Cherukuri, Nagaraj Batta, Dr. Xiaoyu Chen, Dr. Zhihong Mai, Kai Niu, Haifeng Zhang, Jinbo Hou, Yaoxuan Han, Kaijun Yi, Dr. Hao Lin, Dr. Yunshen Zhou, Hao Wang, James HUGHENIN-LOVE, Dr. Zhenyu Yang, Xiaokang Shen, and Jian Chao Li.

I also feel greatly indebted to my entire family, including my wife, my parents, and

my brother. Especially, I would thank my wife Linna. When I felt dismal and encountered difficulties, she always backed me up and gave me all the comforts I needed. She was also my faithful reader and helped me with tons of proof-readings. Without her supports for all these years, I know it will be way much harder for me to get through the entire PhD studies.

Lastly I would like to express my appreciation to the national science foundation (NSF) (grant number:DMI 0555884 and ECS 0629280), the NSF MRSEC at the University of Nebraska-Lincoln, and the Nebraska Research Initiative, for financial support of my research projects.

PREVIEW

TABLE OF CONTENTS

ABSTRACT.....	ii
DEDICATION.....	iii
ACKNOWLEDGEMENTS.....	iv
TABLE OF CONTENTS.....	vi
LIST OF FIGURES.....	ix
LIST OF TABLES.....	xiv
Chapter 1 Introduction.....	1
1.1 Background and motivation.....	2
1.2 Dissertation outline.....	4
Chapter 2 Background and Reviews.....	5
2.1 Introduction to laser-assisted chemical processing.....	6
2.1.1 Laser-assisted photochemical processing.....	6
2.1.2 Near-field induced photochemical process.....	9
2.2 Introduction to diamond-like carbon.....	11
2.2.1 Diamond-like carbon and its general properties.....	11
2.2.2 Conventional techniques in diamond-like carbon synthesis.....	11
2.3 Introduction to carbon nanotube.....	12
2.3.1 Carbon nanotube and its properties.....	12
2.3.2 Synthesis of carbon nanotubes.....	14
2.3.3 Current Problems in CNT Growth/Application.....	16
Chapter 3 Near-Field Controlled and Spatially-Confined Deposition of Diamond-Like Carbon Films on Nanostructures	17
3.1 Introduction.....	18
3.2 Numerical calculation of near-field effects in laser interactions with nanostructures	

.....	19
3.2.1 Local field enhancement at the vicinity of nanotips	19
3.2.2 Local field enhancement at the edges of other nanostructures	22
3.3 Excimer Laser-assisted DLC coating on nanotips	24
3.3.1 Laser deposition of DLC from liquid benzene	24
3.3.2 Laser-assisted chemical vapor deposition of DLC from benzene vapor	24
3.4 Effect of tip-sharpness on phase variation of DLC films at apexes.....	29
3.5 Phase-graded DLC films on a single tip	32
3.6 DLC film deposition on molybdenum nanowedges	36
3.7 Conclusions.....	40
 Chapter 4 Laser-Assisted Pulverization of Nickel Sulphate as Catalyst for Large-Area Synthesis of Carbon Nanotubes	42
4.1 Introduction.....	43
4.2 Laser pulverization of NiSO ₄ micro-clusters.....	45
4.3 Mechanisms of laser-induced pulverization of NiSO ₄	52
4.4 Catalytic growth of CNTs/CNFs	56
4.5 Conclusions.....	62
 Chapter 5 Laser-Assisted Chemical Vapor Deposition of Carbon Nanotubes /Nanofibers.....	63
5.1 Introduction.....	64
5.2 Experimental	65
5.2.1 Substrates	65
5.2.2 Catalyst preparation	65
5.2.3 LCVD system and processes	67
5.3 LCVD Catalytic growth of CNFs/CNTs.....	69
5.3.1 Synthesis of vertically-aligned CNF arrays	69

5.3.2 Synthesis of MWNTs Mats.....	71
5.3.3 Synthesis of suspended SWNTs from Fe/Mo nanoporous islands	73
5.3.4 Synthesis of suspended-CNTs on inverse-Si opal patterns.....	76
5.3.5 Observation of temperature gradient dependent CNT structures	79
5.3.6 Other LCVD experimental parameters on CNT synthesis	82
5.4 Growth mechanisms of carbon nanotubes by LCVD	83
5.4.1 Vapor-liquid-solid model in LCVD growth of carbon nanotubes	83
5.4.2 Effects of catalyst and temperature on CNFs/CNTs.....	86
5.4.3 Effect of laser-induced temperature gradient on structures of CNTs	88
5.5 Conclusions.....	92
Chapter 6 Laser-Assisted Chemical Vapor Deposition for Direct Fabrication of Single-Walled Carbon Nanotube Field-Effect Transistors	94
6.1 Introduction.....	95
6.2 Aligned growth of swnts bridging two electrodes	97
6.2.1 Experimental setup.....	97
6.2.2 Rational for electrical field directed growth	98
6.2.3 Aligned growth of SWNTs bridging two electrodes	100
6.3 Structure characterization of as-grown SWNTs	104
6.3.1 Raman spectroscopy	104
6.3.2 AFM characterization	106
6.4 Electrical transport of CNT FETs	109
6.4.1 Issues about electrical transport in a CNT-FET	109
6.4.2 I-V characteristics	111
6.4.3 Electrical cutting of metallic and semiconducting SWNTs	114
6.5 Conclusions.....	117
CHAPTER 7 Conclusions	118
REFERENCES.....	122

LIST OF FIGURES

Fig. 2.1 Schematic diagram for photo-thermal and photochemical reactions.	8
Fig. 2.2 The unrolled honeycomb lattice of a nanotube with chiral vectors (n,m). General carbon nanotubes include zigzag, armchair, and chiral tubes.....	13
Fig. 2.3 Calculated one-dimensional electronic density of states for a (9,0) nanotube (a) and a (10,0) nanotube (b). The (9,0) nanotube is metallic. The (10,0) nanotube is semiconducting.	14
Fig. 3.1 HFSS model of laser irradiation on a W tip in a benzene environment.	19
Fig. 3.2 Cross-sectional view of the simulated E-field distribution around the apex vicinity. The incident wave direction is along Y axis. The cone is the tungsten tip, enclosed in a rectangular benzene box. (a) ZY cross-sectional view of a tip with a curvature radius of 10 nm, an aspect ratio of 3. (b) ZX cross-sectional view of the same setup as (a). (c) ZX cross-sectional view of a tip with a curvature radius of 70 nm, an aspect ratio of 3, and (d) ZX cross sectional view of a tip with a curvature radius of 100 nm, an aspect ratio of 1.	21
Fig. 3.3 3-D plot of the simulated E-field enhancement factor as a function of tip curvature radius and aspect ratio.....	22
Fig. 3.4 (a) nano-gear modeled in HFSS, the laser incident direction is z direction and the light is polarized at x direction ; (b)-(c) power density distribution on different x-y cross-sections of the nanogear.	23
Fig. 3.5 Experiment setup. (a) Laser deposition in liquid benzene in atmosphere. (b)Laser deposition in a LCVD chamber.	25
Fig. 3.6 (a) Tip curvature radius 650 nm, aspect ratio 3, fluence 6640 mJ/cm ² ; (b) Tip curvature radius 500 nm, aspect ratio 3, fluence 5550 mJ/cm ² ; (c)TEM micrograph, tip curvature radius 20 nm, aspect ratio 1.5, fluence 150 mJ/cm ²	27

Fig. 3.7 SEM micrographs of the tungsten tips after laser irradiation in benzene solution (a) tip 1 with a curvature radius of 100 nm, aspect ratio of 3 under a laser fluence of 187 mJ/cm²; (b) tip 2 with a curvature radius of 153 nm, aspect ratio of 3.5 under a laser fluence of 230 mJ/cm²; and (c) tip 3 with a curvature radius of 480 nm, aspect ratio of 2 under a laser fluence of 230 mJ/cm²..... 30

Fig. 3.8 (a) SEM Micrograph of a W tip before and after laser irradiation; (b) an enlarged scope of view of (a); (c) an enlarged scope of view of (b). The labeled arrows indicate positions where were taken for DLC films were examined by Micro-Raman spectroscopy. 33

Fig. 3.9 Raman shift of the DLC films at different positions on W tip shown in Fig. 3.8 (c) 34

Fig. 3.10 Focused ion beam machined Mo nanowedges. The curvature radii of the nanowedges were about 50 nm in diameter..... 36

Fig. 3.11 SEM micrographs of DLC coating on nanowedges. (a)- (c) Mo nanowedge before deposition. (b), (d) Mo nanowedge after deposition. After DLC coating, top surfaces of the nanowedges were smoothened and the curvature radii increased. 37

Fig. 3.12 (a) Optical microscope image of the electrodes containing nanowedges. Points 1 and 2 indicate the positions of Argon ion laser beam for two consecutive Raman spectroscopy measurements. The rectangle indicates the approximate size of the laser beam; (b) SEM Mo nanowedges contained in the rectangle in (a); Raman spectroscopy at points 1 and 2. 38

Fig. 4.1 (a) Nickel sulphate (NiSO₄·6H₂O) crystal; (b) Micro-clusters on the substrate after substrate immersed in NiSO₄ solution and blown dry by compressed air..... 46

Fig. 4.2 Experimental setup of (a) laser pulverization of NiSO₄ clusters by focused excimer laser; (b) hot-filament CVD system for CNT/CNFs growth..... 47

Fig. 4.3 SEM micrograph of laser-irradiated samples with difference fluences of (a)-(b) 100 mJ/cm², (c)-(d) 200 mJ/cm², and (e)-(f) 300 mJ/cm². Pulse numbers were fixed at 30

pulses. The inset of (f) is an AFM image of nanoparticles in light grey islands shown in (f)..... 48

Fig. 4.4 Statistical analysis of particle size distribution as a function of laser fluence. Pulse number and pulse frequency were fixed at 30 and 5 Hz, respectively. Histograms of size distributions of (a) 100 mJ/cm²; (b) 200 mJ/cm²; (c) 300 mJ/cm²; and (d) average size of particles as a function of laser fluence. 49

Fig. 4.5 SEM micrograph of a sample laser irradiated at 300 mJ/cm². (a)- (b) 5 pulses; (c) 15 pulses; the inset of (c) is a micrometer-sized particle under laser irradiation; (d) average size of particles as a function of pulse numbers. 50

Fig. 4.6 Simulated temperature rise on silicon surface as a function of time under excimer laser irradiation. 55

Fig. 4.7 (a)-(d) SEM micrographs of HFCVD synthesized carbon nanotubes/nanofibers. (a) 100 mJ/cm²; (b) 200 mJ/cm²; (c)-(d) 300 mJ/cm²; (e)-(f) SEM micrographs of LCVD synthesized carbon nanotubes/nanofibers. (e) as-dispersed NiSO₄ clusters; (f) 300 mJ/cm², the inset is a magnified SEM of (f). 57

Fig. 4.8 (a) TEM micrographs of carbon nanofibers grown on samples laser irradiated at 200 mJ/cm², 30 pulses; (b) selected area electron diffraction pattern obtained in (a); (c) TEM micrographs of carbon nanotubes from 300 mJ/cm², 30 pulses; (d) converged beam electron diffraction pattern of area pointed in (c), with a probe size of 8 nm. 58

Fig. 4.9 (a) TEM micrograph of a CNF with a Ni nanoparticle at tip; (b) SEM micrograph of thermally-annealed NiSO₄ dispersed on Si substrates in vacuum after 900 °C for 10 min. 61

Fig. 5.1 Catalysts prepared in this study. (a) Vacuum thermally annealed as-dispersed NiSO₄ micro-clusters on silicon substrates; (b) Uniformly-dispersed NiSO₄ nanoclusters by excimer laser pulverization; (c) Fe/Mo nanoporous catalyst islands; (d) sputtering of thin NiFe films (1 nm) directly on patterned substrates. 67

Fig. 5.2 Laser-assisted chemical vapor deposition system. 68

Fig. 5.3 SEM micrographs of vertically-grown CNFs (a) CNFs grown from circularly dispersed NiSO_4 catalyst particles, (b) close-up view of (a).	70
Fig. 5.4 SEM micrographs of LCVD growth of MWNT/CNF mat through catalysts prepared by laser pulverization. (a) large-area of densely covered MWNTs mat; (b) a close-up view of (a); (c) HRTEM micrograph of MWNTs.	72
Fig. 5.5 (a) SEM micrograph of SWNTs grown from Fe-Mo porous catalyst islands; (b) a long 6- μm SWNT connecting two islands; and (c) TEM micrograph of two twisted SWNTs.	75
Fig. 5.6 SEM micrographs of suspended-SWNT networks span from edges of Si inverse-opal structures. (a) shallow crater; (b) hemispherical crater; (c) protrusions on craters; (d) hollow sphere and frustrum.	77
Fig. 5.7 SEM micrographs of MWNTs creeping on the side surfaces of the inverse-opal structures.	78
Fig. 5.8 Raman spectra of suspended SWNTs and crawling MWNTs excited by a laser at 514.5 nm.	79
Fig 5.9 (a) A sample under laser irradiation with Fe-Mo catalysts. Areas 1-4 are labeled from the center to the position far away from the laser beam. Laser power 35 W, beam diameter 2 mm. Sample size around 20 mm^2 . (b)-(e) SEM micrographs of the morphologies of the corresponding regions labeled in (a).	81
Fig. 5.10 Schematic diagram of the VLS model in a LCVD process.	85
Fig. 5.11 Calculated temperature spatial distributions under a focused CO_2 laser irradiation. SWNT growth threshold temperature defines the boundaries for local synthesis.	91
Fig. 6.1 Setup for electrical-field directed LCVD growth of SWNTs to bridge electrodes.	98
Fig. 6.2 Electrical field induce a directing force to align CNT in the direction of the E-	

field	99
Fig. 6.3 (a) SEM micrograph of patterned Mo electrodes. Circle 'A' is the typical unfocused 2 mm	101
Fig. 6.4 SEM micrograph of two SWNTs bridging the electrodes synthesized by a focused CO ₂ laser beam with a beam size of 340 μ m in diameter.	102
Fig. 6.5 SEM micrograph of SWNTs synthesized using CW Nd:YAG laser.	103
Fig. 6.6 Raman spectroscopy of SWNTs shown in the inset [Fig. 6.3(c)].	105
Fig. 6.7 Raman spectroscopy of SWNTs shown in the inset [Fig. 6.5].	105
Fig. 6.8 AFM images of SWNTs on the SiO ₂ /Si substrate. (a) Phase image of an area of 8 by 8 micron with both electrodes and SWNTs; (b) Topographic image of SWNTs shown in dashed square in (a); Cross-sectional view of a SWNT on the substrate.	107
Fig. 6.9 AFM images of SWNTs grown out of nanocatalysts from a Mo electrode. (a) Phase image; (b) Topographic image of SWNTs shown in dashed square in (a); Cross-sectional view of a SWNT on the substrate.	108
Fig. 6.10 (a) Schematic of a SWNT FET. (b) Band diagram of a p-type SWNT FET. The contacts are Schottky contacts.	111
Fig. 6.11 SEM micrograph of a back-gated 10- μ m long SWNT FET containing a single SWNT as the electron transport channel.	112
Fig. 6.12 (a) <i>I-V</i> curve of a 10- μ m long p type SWNT FET. V_{DS} in the range of -3 to 3 V, V_G -2 to 4 V; (b),(c) band diagrams for positive and negative drain bias	113
Fig. 6.13 Electrical cut of SWNTs. (a) At $V_G = -2$ V, when V_{DS} increased from 0 to 5 V, a metallic-like SWNT was cut; (b) at $V_G = -2$ V, V_{DS} increased from 0 to 8 V (scanned at the second time), the remaining one semiconducting SWNT was also cut.	116

LIST OF TABLES

TABLE 2.1 Laser chemical depositions of various materials.	7
TABLE 3.1. Curvature radii, aspect ratios and laser fluences for different tips.....	31
TABLE 3.2 Fitting parameters of Raman spectra at different positions along the tip, corresponding to the arrows shown in Fig. 3.2(c). Note that points b1 and b2 correspond to the position on the back of the tip which are 1.5 and 4 μm away from apex.	35
TABLE 3.3 Fitting parameters of Raman spectra at different positions along the Mo electrodes, corresponding to the arrows shown in Fig. 3.12(a).	38
TABLE 4.1 EDX elemental analysis of laser disintegrated NiSO_4 compound with 30 pulses at varied laser fluences.....	53
TABLE 5.1 Material properties used in the temperature profile calculation for a three- layer structure under laser beam.	90
TABLE 6.1 List of work functions of several metals and SWNT and the operation types of SWNT-FET using these metals as contacts.....	110

CHAPTER 1

INTRODUCTION

1.1 Background and motivation

1.2 Dissertation outline

1.1 Background and motivation

Since the advent of lasers in the 1960s, laser material processing has become an expanding field and been well established in a wide variety of industrial applications. Some of the mature areas include laser welding, soldering, drilling, and cutting in laser mechanical technology,^{1,2} laser hardening, rapid solidification, glazing, cladding, and powder metallurgy in laser metals technology,^{2,3} and laser recrystallization, doping, and annealing in semiconductor technology.^{4,5} Owing to its unique features, laser technology provides flexibility and precision in material processing in automotive, aviation, medical instrument, and electronics industries. Tremendous research efforts have also been made in advancing laser material processing in microelectronic, data storage, and photonic applications. However, for a very long time, the inherent diffraction limit of laser wavelengths has constrained applications of conventional laser material processing in nanotechnology. To achieve nanoscale laser material processing, it is imperative to overcome the diffraction limit, which can only be realized by fundamental scientific innovations.

Currently, there are several important research directions, in which intensive laser nanoprocessing studies are being carried out: 1) to develop short wavelength optical source and optics, down to X-ray range⁶⁻⁹; 2) to develop ultrafast laser machining with current advances in femtosecond to future attosecond laser processing;¹⁰⁻¹² 3) to develop near-field related optical nanoprocessing, which is one of the most promising directions for next-generation nanolithography;¹³⁻¹⁸ and 4) to develop laser techniques utilizing nanopatterns for nanoimprinting.¹⁹⁻²¹ Most of these techniques address material removal or substrate patterning with high precision and controllability at nanoscales. Although it is of significant research and practical value, highly-controlled deposition of materials on nanostructures is rarely studied and many fundamental phenomena are yet to be explored. As a result, there are tremendous research needs in developing advanced techniques for high-quality nanoscale material synthesis and deposition with a high controllability in the material property as well deposition positions.

In this dissertation, our endeavours are extended to explore the capability of

laser-based nanoprocessing techniques for controlled deposition and synthesis of nanoscale materials, such as diamond-like carbon films, and carbon nanotube/carbon nanofiber structures. In addition, fundamental understandings of the process mechanisms and their implications were also systematically studied. Within the framework of this objective, the research projects mainly focused on using laser for nanoscale material synthesis, including: 1) laser-assisted deposition of diamond-like carbon films on nanotips and nanowedges induced by near-field photochemical processing; 2) laser chemical vapor deposition (LCVD) of carbon nanotubes and carbon nanofibers, which was further applied to the fabrication of carbon nanotube field-effect transistors.

The research projects have the following significances in terms of academic contribution and industrial impact. For the study of near-field-induced position-controlled DLC coating on nanostructures, 1) it is a controllable surface process which extends surface coating to nanoscales in three dimensions, which bears major scientific interests in fundamental research; 2) it is a technique directly addressing the needs for coatings on sharp tips and edges of nanostructures, especially as self-lubricating and protective coatings for extensive wear applications at nanometric levels. For CNT growth using LCVD techniques, we not only established an independent CNT growth technique for high-speed, position-controlled CNT growth. In addition, this technique has successfully been applied to the fabrication of field-effect transistors, which bears great potential for electronic property control during growth by CNT-chirality selection.

1.2 Dissertation outline

This dissertation focuses on applying laser-based physical/chemical processes to nanoscale material processing and device fabrication. The entire dissertation is divided into seven chapters. In chapter 1, the motivation of this project and the dissertation outline are introduced. Chapter 2 elucidates the background and history of three important aspects of this project: 1) laser-assisted chemical processing, 2) diamond-like carbon material (properties, preparation, and applications), 3) carbon nanotube material (properties, synthesis, applications, and current limitations). Chapter 3 describes film deposition of diamond-like carbon on nanostructures controlled by laser-induced near fields. Both theoretical and experimental studies on enhanced optical near-field induced photochemical are described. Chapter 4 describes pulsed excimer laser nano-fragmentation of compound particles. This technique was applied to generating highly-uniform nanocatalysts for large-area synthesis of CNTs. Chapter 5 presents laser CVD synthesis of CNTs. In this chapter, a detailed study using CO₂ and Nd:YAG laser for nanofiber/nanotube material is introduced. The mechanisms of LCVD process for CNT growth are also discussed. In chapter 6, we extend LCVD technique in direct fabrication of CNT field effect transistors. The CNT growth can be conducted in a position- and direction-controlled manner. There is great potential in LCVD technique that it can achieve chirality selection during *in-situ* growth, which tackles the biggest challenge for lack of control of chirality-related electronic properties. Chapter 7 concludes this work with a summary of important results.

CHAPTER 2

BACKGROUND AND REVIEWS

2.1 Introduction to laser-assisted chemical processing

2.2 Introduction to diamond-like carbon

2.3 Introduction to carbon nanotube

2.1 Introduction to laser-assisted chemical processing

2.1.1 Laser-assisted photochemical processing

Laser photochemical processing is one of the most active areas in laser material processing, which can efficiently assist etching and thin film deposition via chemical methods. Through laser chemical vapor deposition (LCVD) method, a variety of materials, such as metals (from metal halides, alkyls and carbonyls), semiconductors (amorphous and crystalline Ge, Si, and compound semiconductors), insulators (oxides and nitrides), and heterostructures can be deposited.^{22,23} Table 2.1 summarizes typical materials, their feed-sources and wavelengths for these applications.

Laser light can induce chemical reactions either homogeneously within the gas or liquid phase, or heterogeneously at molecule-solid or solid-solid interfaces. In general, laser chemical processing involves both photothermal and photolytic processes. In photothermal process, multiple photons in the Vis-IR range must be absorbed to elevate the molecules to higher vibration levels until atoms are ionized or molecules are dissociated. In photolytic process, by absorption of UV-Vis photons, molecules can be directly dissociated by electronic dissociation in a single step.

A simple model²², as shown in Fig.2.1, will be used to briefly explain such complex processes. Let A and A^* characterize the system in the ground state and excited state, respectively. By assuming that there is no spontaneous emission, non-radiative transitions $A^* \rightarrow A$ are described by the thermal relaxation time, τ_T . The characteristic time for reaction of A and A^* with C are $\tau_A(T)$ and $\tau_{A^*}(T)$. At low excitation rates, where $\tau_T \leq h\nu / \delta I$ (δ is the excitation cross section), if $\tau_T \ll \tau_{A^*}$ and $\tau_A \ll \tau_{A^*}$, the excitation energy is immediately dissipated into heat and the reaction is thermally activated; if $\tau_T > \tau_{A^*}$ and $\tau_A \ll \tau_{A^*}$, the process is mainly photo-chemically and photolytically activated, during which the reaction takes place via excited species A^* ; if $\tau_T \ll \tau_{A^*}$, τ_A and $\tau_{A^*} \ll \tau_A$, or if all these time periods are comparable, both the 'thermal channel' and the 'photochemical channel' need to be considered.

TABLE 2.1 Laser chemical depositions of various materials.

Deposited material	Carrier gases	Substrate	Laser/wavelength (nm)	Ref.
Ag	AgCF ₃ SO ₃ , AgPF ₆ , AgBF ₄ /C ₆ H ₅ CH ₃	Glass, SiO ₂	HeCD 325	24
Au	Au(CH ₃) ₂ (acac)	Si	Ar 515	25
Au	HAuCl ₄ /aq.	(100)Si	p-Nd:YAG 532	26
Fe	Fe(CO) ₅	Al ₂ O ₃ , (100)	ArF 193, KrF 248	27
Fe	Fe(CO) ₅	GaAs (100)Si	Hg lamp	28
Ni	Ni(CO) ₄ /He	Si	Ar 515	29
Ni	Ni(CO) ₄ /Ar	Glass	CO ₂ 10.6um	30
Si	SiH ₄	SiO ₂	KrF	27
Si	SiH ₄	SiO ₂	CO ₂ 10.6um	31
GaAs	Ga(CH ₃) ₃ +AsH ₃ / H ₂	(100) GaAs	Ar 458-515 ; Nd:YAG 532	32,29
C (diamond)	2%CH ₄ +H ₂	(100)Si ,	CO ₂ 10.6um	33
C (diamond)	0.5%- 2%CH ₄ +H ₂	Si	ArF 193	34,35
C (diamond-like carbon)	C ₆ H ₁₂	Si	KrF 248	36,37

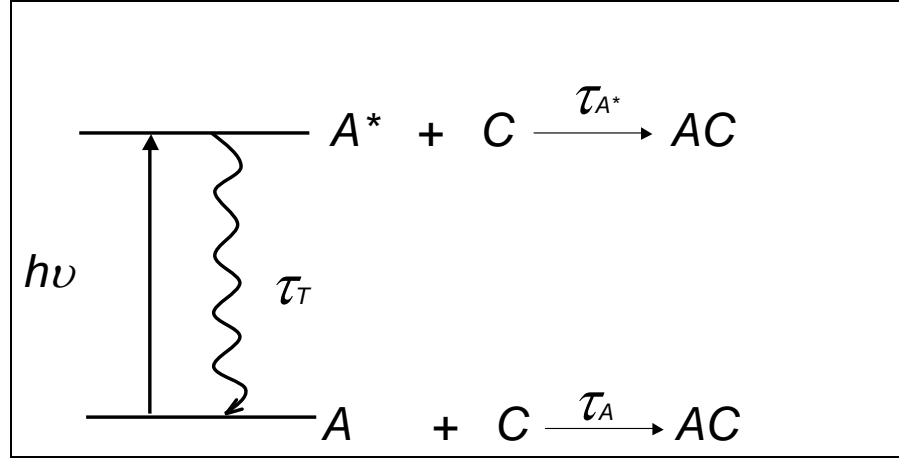


Fig. 2.1 Schematic diagram for photo-thermal and photochemical reactions.

For photo-thermally activated reactions, the net reaction rate can be described by

$$W(x, t) = k(T) N^{\gamma_{AB}}_{AB} N^{\gamma_{CD}}_{CD} \cdots = W_0(x, t) \exp\left(-\frac{\Delta E}{k_B T(x, t)}\right), \quad (\text{Eq. 2.1})$$

where rate constant $k(T) = k_0 \exp\left(-\frac{\Delta E}{k_B T(x, t)}\right)$ follows the Arrhenius law; ΔE is the apparent chemical activation energy; $N^{\gamma_{AB}}_{AB}$ is the density of the species, k_0 is a pre-exponential factor whose dimension depends on the total reaction order; and $T(x, t)$ is the temperature distribution and γ_i is partial reaction order.

For photolytically (photo-chemically) activated reactions the rate

$$W(x, t) = W'_0 \prod_i \left[\sigma_i \left(\frac{I(x, t)}{h\nu} \right)^n \right]^{\gamma_i} = k'(I) N^{\gamma_{AB}}_{AB} N^{\gamma_{CD}}_{CD} \cdots, \quad (\text{Eq. 2.2})$$

where $W'_0 = k'_0 N^{\gamma_{AB}}_{AB} N^{\gamma_{CD}}_{CD} \cdots$, and $k'(I) = k'_0 \prod_i \left[\sigma_i \left(\frac{I(x, t)}{h\nu} \right)^n \right]^{\gamma_i}$, k'_0 and thereby W'_0 depends on the relaxation time relevant for selective excitation of species. Eq. (2.2) denotes the product over all species to be excited. As an example, single-photon excitation with a single type of reactant, AB , which can be characterized by $i=AB$, $n=1$, $\gamma_{AB}=1$,

$\gamma_{CD} = 0$. The rate constant is, $k'(I) = k_o' \sigma_{AB} \frac{I}{h\nu}$, where σ_{AB} is the single-photon excitation cross section. It is found that various gas-molecules have different excitation cross sections under different wavelengths.

2.1.2 Near-field induced photochemical process

Optical near-field theory, especially, light interaction with small particles, sharp tips, and tapered fibers, was developed in recent decades and in particular after the discovery of the surface enhanced Raman scattering (SERS)^{38,39}. In 1980s, many theoretical works were carried out on the SERS phenomenon. It suggested that the enhancement was a result of a number of electrostatics effects,^{40,41} surface plasmon effects⁴² and electrodynamic effects,⁴³ and their combinations.⁴⁴ In brief, the local electromagnetic field that excited molecules adsorbed on a rough surface of some metals could be considerably greater than the field of the primary beam that interacted with the same molecules in the liquid or gas phases.

Based on theories of SERS, scanning near-field optical microscope (SNOM) and apertureless SNOM (photo-assisted scanning probe microscope) were developed to obtain additional information on sample surfaces.^{45,46} It is based on optical-field confinement by surface plasmons of a submicron metal particle. The field extended to a nearby sample surface and was re-radiated by the particle, thereby generating a Raman, a two-photon, or a second-harmonic spectrum. In addition, SNOM and apertureless SNOM have recently aroused great interest in nanoscopy^{47,48} and nanofabrication.^{13,49} The concept is also applicable to submicrometer lithography and ultra-high-density optical recording.⁵⁰

Many studies have also focused on theoretical aspect of optical near-field phenomena in terms of optical field enhancement and effect of nanoparticle, nanotip shapes. Using a small particle model, Dickmann⁵¹ *et al.* evaluated the intensity gain versus tip aspect ratio for different tip materials at a wavelength of $\lambda=532$ nm. A maximum intensity gain of up to 10^6 could be obtained for excellent conducting metals (e.g., gold and silver). However, the estimated value was much larger than the experimental results. Using a quasistatic model, Denk and Pohl⁴¹ presented their